© Indian Academy of Sciences

CrossMark

CFD study of forced convective heat transfer enhancement in a 90° bend duct of square cross section using nanofluid

ASHOK K BARIK*, PRASANTA K SATAPATHY and SUDHANSU S SAHOO

Department of Mechanical Engineering, College of Engineering and Technology, Bhubaneswar 751003, Odisha, India
e-mail: ashokbarik.mech@gmail.com

Abstract. In this paper, the forced convective heat transfer enhancement with nanofluids in a 90° pipe bend has been presented. Numerical investigation is carried out for the turbulent flow through the pipe employing finite volume method. The governing differential equations are discretized using hexahedral cells, and the resulting algebraic equations are solved using Commercial solver Fluent 6.3. In order to close the time averaged Navier–Stokes equations, the two-equation $k–\varepsilon$ turbulence model with a standard wall function have been used. The duct Reynolds number is varied in the range of 2,500–6,000. It is observed that the heat transfer is enhanced significantly by varying the volume fraction of the nanofluid. It is also found that the heat transfer is increased with Reynolds number. A strong secondary flow is observed due to the presence of the wall. Turbulent kinetic energy near outer wall is found to be higher than the inner wall of the bend. A comparative assessment for the heat transfer enhancement with different types of nanofluids is also presented. The computed results of area weighted average Nusselt numbers are validated with some of the existing literature.

Keywords. Nanofluids; $k–\varepsilon$ turbulence model; 90° bend pipe; forced convection.

1. Introduction

Forced convection heat transfer can be enhanced by increasing the thermal conductivity of a fluid medium, which carries the heat along with it. Also, the operating condition is one of the factors that affect the heat transfer rate. Conventional fluids such as oil, water, and ethylene glycol are rather poor heat transfer mediums. The thermal management of the heat transfer equipment demands a high heat transfer rate from a smaller surface area. The designing of thermal equipment is more challenging because of miniaturization of devices. Thus, the attempts have been focused by many researchers [1–3] to optimize the geometry of engineering equipment with a hope to attain a higher thermal efficiency. Now-a-days, the use of the conventional fluids in these miniaturized devices has been replaced with nanofluids. The fluid flow and the heat transfer characteristics of a fluid containing millimeter- or micrometer-sized particles have been studied by different researchers [4–7]. Since these suspended particles are relatively larger in size as compared to the nanofluids, the problems of poor suspension stability, channel clogging and abrasion of tubes are inevitable. However, the fluids with nanometer-sized particles do not suffer these problems; rather have higher thermal conductivity than that of the theoretical predicted

values [8]. The heat transfer enhancement by the nanofluids has been studied comprehensively by Xuan and Li [9], Wang and Majumdar [10], Kakaç and Pramuanjaroenkij [11]. According to these researchers the nanofluids enhance the heat transfer because of (1) increased surface area around nanoparticles in the base fluid, (2) increased thermal conductivity of the mixture (i.e., basefluid + nanoparticle), and (3) intense inter-particle collisions and thermal dispersion.

The convective heat transfer mechanism in nanofluids was studied first by Xuan and Roetzel [12]. They concluded that thermal dispersion and increased thermal conductivity are the major mechanisms to enhance heat transfer rate in nanofluids. Roy *et al* [13] and Palm *et al* [14] numerically studied the convective heat transfer characteristics of nanofluid using single-phase model, and assumed that the nanofluid maintains thermal equilibrium with the base fluid. The turbulent heat transfer performance of nanofluid was studied numerically by Boungiorno [15]. The heat transfer enhancement near-wall layer was based on two region model: the viscous sub-layer and the turbulent sub-layer. The thermal conductivity was dominated over the fluid viscosity and the particle volume fraction in the viscous sub-layer. In this region, the heat transfer enhancement was primarily due to the reduction in the viscosity resulting in a thinner viscous sub-layer due to the nanoparticles. Moreover, the turbulent convective heat transfer of Al_2O_3–water

*For correspondence

nanofluids has been studied numerically in a long horizontal tube by Rostamani *et al* [16].

Anoop *et al* [17] studied the effect of nanoparticle size on heat transfer augmentation. They reported that the small sized nanoparticles (45 nm diameter) were better heat transfer augmenter than the large sized nanoparticles (150 nm diameter). In an experimental study of TiO_2–water nanofluid flowing in a vertical pipe, Heris *et al* [18] observed a reduction in heat transfer enhancement as the size of the nanoparticle was increased. The reduction in the heat transfer enhancement was attributed to the decrease in thermal conductivity of nanofluids with particle size. The laminar convective heat transfer of nanofluids has been studied experimentally by Wen and Ding [19] using a straight copper tube of 970 mm long. The heat transfer enhancement in the developing region of the pipe was found higher. Heris *et al* [18, 20], Seyf and Feizbakhshi [21], Nazififard *et al* [22], Bianco *et al* [23] have studied the effects of nanofluids CuO–water/Al_2O_3–water on the heat transfer rate for laminar or turbulent flow through circular pipes. An experimental investigation for the convective heat transfer enhancement has been carried out by Heris *et al* [24] using of Al_2O_3/water nanofluid flowing in a square duct. They concluded that the poor heat transfer performance of noncircular cross section such as square can be overcome by using nanofluids. They reported that there exists the static fluid region near the corners of the non-circular dusts; and with the use of nanofluid, the nanoparticles can migrate to the sharp corners and effectively dissipate heat from those regions so as to enhance the heat transfer performances.

A two-phase approach has been employed by Lotfi *et al* [25] to investigate the turbulent forced convective heat transfer characteristics of Al_2O_3–water nanofluids flowing in a circular tube. They demonstrated that the two-phase mixture model was able to predict the heat transfer rate in a very precise way. A comparative study has been carried out by Azari *et al* [26] employing different two-phase models of commercial software Fluent. They concluded that the single-phase model was able to predict the heat transfer effectively at low concentration of nanofluids; whereas at high concentration the heat transfer rate matches well with their experimental results. From the above literature review, it is clear that the heat transfer enhancement in 90° bend pipe using Al_2O_3–water nanofluid has not been carried out earlier. As far as authors' knowledge, the present investigation is the first of its kind. Therefore, in the present study, an attempt has been made to carry out the numerical investigation of the effects of the nanofluid volume fraction and the Reynolds number on the heat transfer rate.

2. Mathematical formulation

2.1 *Physical situation and grid arrangement*

The physical model used in the present numerical investigation has been depicted in figures 1(a) and (c). The expanded and cutaway view of the grid arrangement has been illustrated in figure 1(b). Hexahedral cells have been
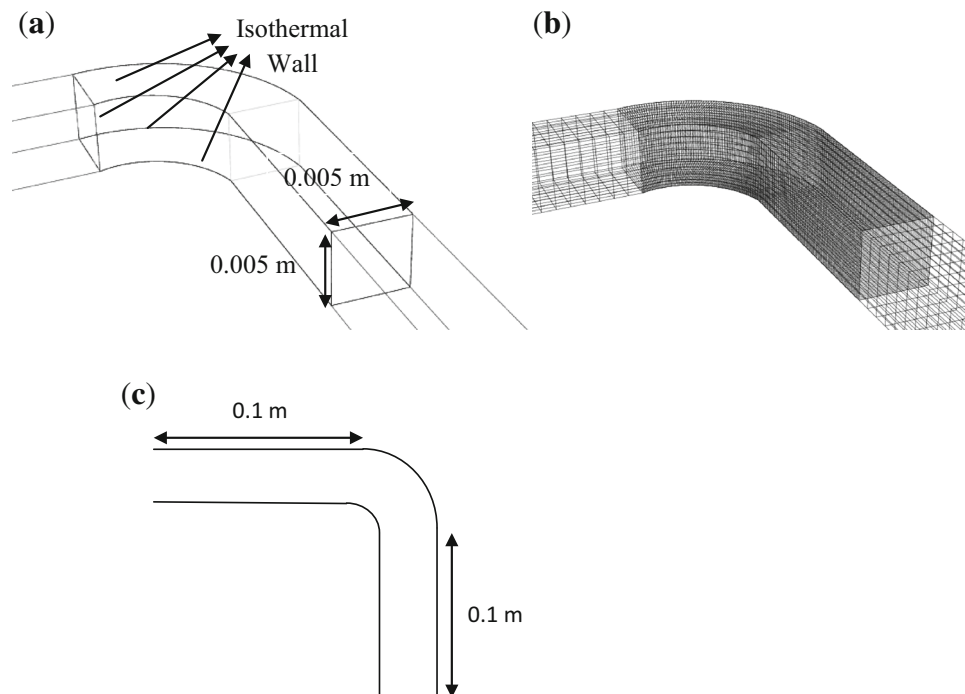

Figure 1. Physical situation and grid arrangement (**a**) Cutaway view of 90° bend; (**b**) Grid arrangement; (**c**) *x–z* plane passing through the 90° bend pipe.

employed to mesh the computational domain. It is seen that finer grids have been used on the bend portion of the pipe since the flow at the bend portion experiences a centrifugal force due to the curvature effect. Therefore, it is expected that the flow attains a higher velocity at the outer wall than the inner wall. Thus, the sharp gradients in the flow variables may be correctly captured by employing finer grids in the bend portion.

2.2 *Governing equations*

The conservation equations for mass, momentum and energy are solved in a three-dimensional computational domain as shown in figures 1(a) and (b). For practical applications, the size of the nanoparticles, in general, is less than 100 nm. Therefore, these finer particles when mixed with the base fluid forms a mixture that can be modelled as a continuous medium like a single-phase fluid such as water [9, 27]. In the present study, the following assumptions have been incorporated into the numerical scheme:

1. The average flow is steady, turbulent and single phase.
2. The slip velocity between nanoparticles and base fluid is negligible, and the thermal equilibrium between the continuous phase and discrete particles is prevailed.
3. The nanofluid is treated as incompressible and Newtonian with constant physical properties.
4. The thermal radiation, viscous dissipation, and compression work are negligibly small in the energy equation. Thus, these terms are neglected.

With these assumptions, the governing equations for the above analysis can be written as

Continuity

$$\rho_{nf}\nabla \cdot \mathbf{v}_{nf} = 0 \qquad (1)$$

Momentum

$$\rho_{nf}\nabla \cdot (\mathbf{v}_{nf}\mathbf{v}_{nf}) = -\nabla p + \nabla \cdot (\bar{\bar{\tau}}) \qquad (2)$$

Energy

$$\rho_{nf}C_{p,nf}\nabla \cdot T_{nf} = k_{nf}\nabla \cdot (\nabla T_{nf}) \qquad (3)$$

where $\bar{\bar{\tau}}$ is the stress tensor. Since constant fluid properties have been used in the present study, thus, the laminar viscosity and thermal conductivity are kept constant. As an isotropic turbulence model (i.e., the standard $k - \varepsilon$ turbulence) is used, the modified pressure, 'p' in Eq. (2) will scramble to be $(p + 2k\rho_{nf}/3)$, which is computed iteratively from the momentum and continuity balance using the SIMPLE algorithm.

The stress tensor $\bar{\bar{\tau}}$ is given by

$$\bar{\bar{\tau}} = \mu_{nf}^{eff}\left(\nabla \mathbf{v}_{nf} + \nabla \mathbf{v}_{nf}^T\right) \qquad (4)$$

Effective viscosity, $\mu_{nf}^{eff} = (\mu_{nf} + \mu_{t,nf})$ Turbulent viscosity, $\mu_{t,nf}$, computed from $\mu_{t,nf} = \rho_{nf}C_\mu\frac{k^2}{\varepsilon}$

Turbulent kinetic energy (k)

$$\nabla \cdot (\rho_{nf}v_{nf}k) = \nabla \cdot \left(\frac{\mu_{t,nf}}{\sigma_k}\nabla k\right) + G_{k,nf} - \rho_{nf}\varepsilon. \qquad (5)$$

Dissipation rate (ε)

$$\nabla \cdot (\rho_{nf}v_{nf}\varepsilon) = \nabla \cdot \left(\frac{\mu_{t,nf}}{\sigma_\varepsilon}\nabla \varepsilon\right) + \frac{\varepsilon}{k}\left(C_{1\varepsilon}G_{k,nf} - C_{2\varepsilon}\rho_{nf}\varepsilon\right). \qquad (6)$$

The term $G_{k,nf}$ represents the production of turbulent kinetic energy and is computed from

$$G_{k,nf} = \mu_{t,nf}\left(\nabla \mathbf{v}_{nf} + (\nabla \mathbf{v}_{nf})^T\right) : \nabla \mathbf{v}_{nf} \qquad (7)$$

σ_k, σ_ε are Prandtl's numbers for k and ε. $C_{1\varepsilon} = 1.44, C_{2\varepsilon} = 0.09, \sigma_k = 1.0, \sigma_\varepsilon = 1.3, C_\mu = 0.09$

$Pr_t = 1$. To link the solution variables at near-wall cells and the corresponding quantites on the wall, a standard wall function has been employed as proposed by Launder and Spalding [28]. Barik *et al* [29, 30] used k–ε turbulence model along with the standard wall function to model the air entrainment into an infrared suppression device (IRS). The law-of-wall for mean velocity is given as

$$\frac{\rho_{nf}u_p k_p^{1/2}c_{\mu,nf}^{1/4}}{\tau_w/\rho_{nf}} = \frac{1}{\kappa}\ln(Ey^*) \qquad (8)$$

$$y^* = \frac{\rho_{nf}k_p^{1/2}c_{\mu,nf}^{1/4}y_p}{\mu_{nf}} \qquad (9)$$

$E =$ empirical constant $= 9.793$, $\kappa =$ von Karman constant $= 0.4187$, $u_p =$ mean velocity of fluid at point 'P', and $\tau_w =$ the wall shear stress. The turbulent intensity at the duct inlet has been calculated from $I = 0.016\mathrm{Re}^{-(1/8)}$.

2.3 *Boundary conditions*

Since Eqs. (1)–(3) are elliptic, nonlinear and coupled partial differential equations; an iterative solution method has been adopted to solve the unknown variables by imposing appropriate boundary conditions. At the duct inlet, the velocity inlet boundary condition has been imposed. A uniform axial velocity u_{in}, temperature T_{in} (which is equal to T_o) has been specified at the inlet. At the pipe outlet, the outflow boundary condition has been applied. The outflow boundary condition ensures that there would be no back flow at the pipe outlet. It is expected that the flow is hydrodynamically fully developed before reaching the bend portion of the conduit. For turbulent flows, it has been well established that the hydrodynamic entry length for most of the practical engineering applications is about 10 times the

hydraulic diameter of the conduit. In the present study, a length of the conduit 20 times the hydraulic diameter ($x/D_h = 20$) has been considered, so that flow is expected to develop fully (hydrodynamic) at the entrance of the bend. However, it is worth mentioning here that the flow may not be fully developed at the outlet section of the conduit due to the presence of the bend. Recently, the finite element method has been employed by Choi and Zhang [31] to investigate the heat transfer characteristics of circular return bend tube using nanofluids. The lengths of the straight portion of the tube before and after the return bend are 10 times the dimensionless diameter. Since the present investigation is concerned about the thermo-hydraulic characteristics of 90° bend; thus, the inlet and outlet portions of the 90° bend are subjected to adiabatic boundary condition. A constant temperature ($T_w = 363K$) has been applied to the walls of the bend. The mathematical descriptions of different boundary conditions used in the present computational study are given as follows:

$$\text{Pipe inlet:} \quad v = w = 0, \ u = u_{in}, \ T = T_{in} = T_0 \quad (10)$$

$$\text{Pipe outlet:} \quad \frac{\partial ()}{\partial n} = 0, \quad (11)$$

where n is the outward normal drawn to the pipe outlet. At the pipe outlet, the pressure outlet boundary condition has been imposed since atmospheric pressure is prevailed.

$$\text{Adiabatic walls of the pipe:} \quad u = v = w = 0,$$
$$\frac{\partial T}{\partial x} = \frac{\partial T}{\partial y} = \frac{\partial T}{\partial z} = 0, \quad (12)$$

$$\text{Constant temperature bend walls:} \quad u = v = w = 0,$$
$$T_x = T_y = T_z = T_w \quad (13)$$

2.4 *Physical properties for nanofluid*

The nanoparticles are assumed to be dispersed well in the base fluid. Therefore, the thermo-physical properties of nanofluid are evaluated from some classical well-known formulas for single phase constant property fluids. Different thermo-physical properties of Al_2O_3 nanoparticle as well as water (i.e., base fluid) are given in the table 1. The subscripts p, bf and nf represents the nanoparticle, base fluid

Table 1. Thermo-physical properties Al_2O_3 nanoprticle and water.

Properties	Al_2O_3-nanoparicles (p)	Water (bf)
Density, ρ (kg/m^3)	3880	998.2
Thremal conductivity, k(W/ m − K)	36	0.597
Sp. heat, c(J/kg −K)	773	4182
Viscosity (kg/m − s)	–	9.93×10^{-4}

and nanofluid, respectively. In the present study, the temperature independent, and the volume fraction dependent densities for Al_2O_3–water nanofluid have been employed. The volume fraction dependent density for nanofluid is calculated from Eq. (14) as has been suggested by different researchers [23, 32]:

$$\rho_{nf} = (1 - \phi)\rho_{bf} + \phi\rho_p \quad (14)$$

The above formula commonly used for obtaining the nanofluid density has been obtained from experimental results of Pak and Cho [33]. The dynamic viscosity of Al_2O_3–water nanofluid has been evaluated from the classical homogenous two-phase mixture model neglecting the slip velocity between the phases as given in the following equation.

$$\mu_r = \frac{\mu_{nf}}{\mu_{bf}} = 123\phi^2 + 7.3\phi + 1. \quad (15)$$

A least square analysis had been carried out by Maiga *et al* [34] to fit the experimental data of the researchers [35] to obtain the above equation. The specific heat of the mixture is obtained from Eq. (16) as has been reported by different researchers [27, 36].

$$c_{nf} = (1 - \phi)c_{bf} + \phi c_p. \quad (16)$$

The same criteria as that of the viscosity have been used to determine the thermal conductivity of the nanofluid. The thermal conductivity is determined from the following equation.

$$k_r = \frac{k_{nf}}{k_{bf}} = 4.97\phi^2 + 2.72\phi + 1. \quad (17)$$

The above thermal conductivity model assumes that the nanoparticles are spherical in shape which is may not be the case in a real situation. Thus, this model under-predicts the thermal conductivity of nanofluids. However, this model is very simple and easy model to implement in the numerical computations. Therefore, we have used this model to evaluate the thermal conductivity of Al_2O_3–water nanofluid. Before proceeding to the validation of the present numerical methodology, the area weighted average Nusselt number, local Nusselt number, bulk mean temperature and the Reynolds number based on the hydraulic diameter of the duct are given as follows:

The area weighted average Nusselt number:

$$\overline{Nu}_{Dh} = \frac{1}{A} \int Nu_{Dh} dA. \quad (18)$$

The local Nusselt number is computed as

$$Nu_{Dh} = \frac{h_w D_h}{k_{nf}}, \quad (19)$$

where the local heat transfer coefficient, $h_w = q_w/(T_w - T_b) = (k_{nf}(\partial T/\partial r)|r = 0)/(T_w - T_b)$, and r, is the coordinate direction in y and z, respectively. The

bulk mean temperature in the computational domain is computed from the local temperature, T according to the following equation.

$$T_b = \frac{1}{A} \int T dA. \tag{20}$$

In Eq. (18), dA is the cross-sectional area. All properties are calculated from the bulk temperature.

$$\text{Re}_{Dh} = \frac{\rho_{nf} u_{in} D_h}{\mu_{nf}}. \tag{21}$$

3. Numerical solution procedure

Hexahedral cells have been deployed to discretize the three-dimensional computational domain. A faster convergence rate and better solution accuracy are achieved with the hexahedral cells since the flow is aligned with the cell faces. Conservation equations for mass, momentum, and energy are integrated over the control volume to yield a set of algebraic equations. The second order upwind scheme is used for the convective terms [25, 26], and central difference scheme which is always second order accurate has been employed to discretize the diffusion terms. A short description of the second order upwind scheme has been given for reference. In a second order upwind scheme, the face value (φ_f) is computed as $\varphi_f = \varphi + \nabla\varphi . \overrightarrow{r}$. φ, denotes the cell centered value with its upstream gradient is $\nabla\varphi$, and $\overrightarrow{r}$ represents the displacement vector from upstream cell centroid to face centroid. $\nabla\varphi$, at cell centroid is computed as $\nabla\varphi = \frac{1}{v}\sum_f \overline{\varphi}_f A_f$. φ_f, is the value of φ at the face centroid, and is computed from the Green–Gauss node based gradient evolution as $\overline{\varphi}_f = \frac{1}{N_f}\sum_n^{N_f} \overline{\varphi}_n$, $\overline{\varphi}_f =$ the

arithmetic average of node values on a face, N_f is the number of nodes on the face, and $\overline{\varphi}_n$ is calculated from a weighted average of cells surrounding a node. A staggered grid layout has been employed to compute the temperature and velocity components at the center of control volume interfaces. SIMPLE (Semi-Implicit Method for Pressure-Linked Equations) algorithm has been employed for pressure–velocity coupling to solve pressure correction equation. The algebraic equations are then solved iteratively using a point implicit (Gauss–Siedel) linear equation solver in conjunction with algebraic multi-grid solver of Fluent 6.3 by incorporating the boundary conditions. The under relaxation factors (for pressure = 0.3, momentum = 0.7, energy = 1, turbulent kinetic energy and its dissipation rate = 0.8 each) have been used to update solution variables at the end of each iteration. The solutions are found to converge, when the residuals resulting from the iterative solutions fall below 10^{-4} and 10^{-7} respectively for momentum and energy equations.

4. Validation of numerical methodology

Attempts have been made to validate the present numerical scheme with some of the existing literature. It is worth mentioning here that there exist neither experimental nor numerical data to validate the heat transfer from a 90° bend pipe of rectangular cross section carrying Al_2O_3–water nanofluid. Therefore, the authors have tried their best to validate the present numerical models with some of the correlations given by Pak and Cho [33] as well as Maiga *et al* [27] as shown in figure 2(a). It is observed from figure 2(a) that the Nusselt number increases linearly with the duct Reynolds number. A similar trend has been captured by our numerical scheme. The present computed Nusselt numbers little higher than the results reported by Pak and Cho [33].

This is due to the fact that the Al_2O_3 nanofluid has been used in the present computation; whereas TiO_2, whose
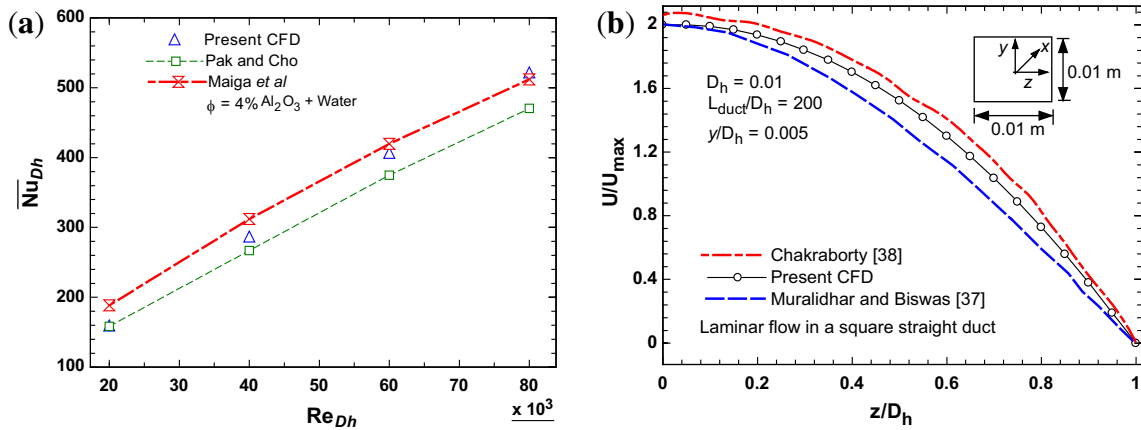

Figure 2. (a) Variation of average Nusselt number with duct Reynolds number; (b) Variation of velocity along radial direction at outlet of square duct.
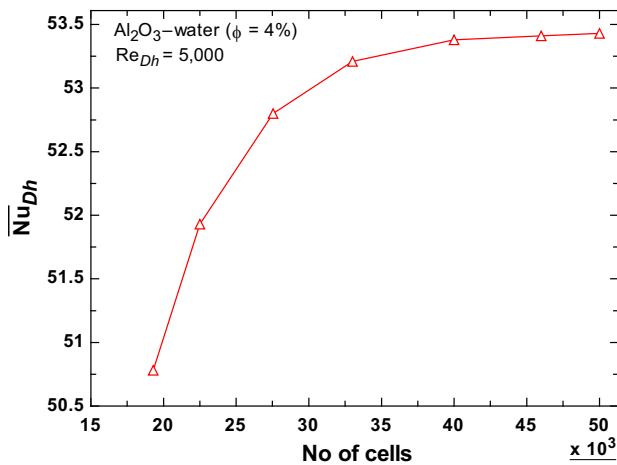
Figure 3. Grid independence test.

Figure 4. Variation of average Nusslelt number with Reynolds number of the duct.

thermal conductivity is lower than that of the Al_2O_3, nanofluid was used by Pak and Cho [33]. It is also observed that the computed values of the Nusselt number matches well with the results obtained by Maiga *et al* [27]. Figure 2(b) shows the validation of the present CFD results with the analytical results of Muralidhar and Biswas [37] as well as Chakraborty [38]. It has been noticed from figure 2(b) that the CFD results matches reasonably with the analytical results. Laminar flow in a square duct has been taken for the present validation. Thus, it is ascertained that the present numerical schemes are capable of predicting the heat transfer as well as flow characteristics in non-circular ducts, and are implemented in the present study.

5. Results and discussions

5.1 *Grid independence test*

The grid independence test for the present work has been shown in figure 3. The computation has been started initially with 19,200 cells. The computed Nusselt number was 50.78. The grids are refined subsequently to increase the number of cells to 33,000 and the Nusselt number by that time was 53.21, which register a change in Nusselt number 4.78%. Thereafter, the number of cells has been increased to 50,000, which register a change in Nusselt number 0.375%. Therefore, a computational domain containing number of cells of 33,000 have been used for our further analysis. At 33,000 cells, the y^+ value is noticed within the limit of $30 < y^+ < 300$, which is a required condition for the use of the standard wall function. In the present case the y^+ value lies in the range of 50–148 for the hot wall where we have incorporated fine meshes in order to capture the sharp gradients in the flow variables.
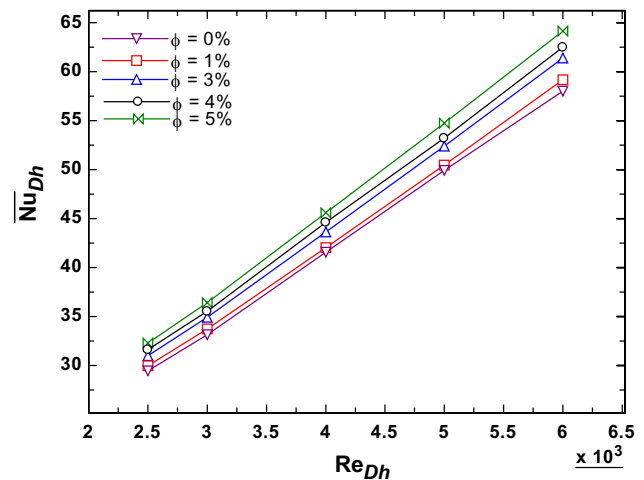
5.2 *Effect of Reynolds number on heat transfer enhancement*

The effect of Reynolds number on heat transfer enhancement for Al_2O_3–water nanofluid is shown in figure 4. At a particular volume fraction of the nanofluid, the average Nusselt number is observed to increase monotonously with the Reynolds number. It is quite obvious that the heat transfer rate to the fluid increases with the Reynolds number, as a more amount of heat is carried by a faster moving fluid than a slower moving fluid; and as a result of this, the Nusselt number has been increased with the Reynolds number. The same phenomena have been shown by the nanofluid.

At a particular volume fraction and Reynolds number, the velocity contours (expanded and cutaway view) are shown in figure 4 to explain the fluid flow characteristics. The occurrence of secondary flow in the bend duct has been shown in the sub-figure of figure 5. For the sake of clarity, the velocity vector has been shown in a single plane (as shown by an arrow mark in figure 5). It is seen from the sub-figure of figure 5 that two counter rotating vertices are developed which are thought to be the direct consequence of the effect of centrifugal force on the bulk fluid motion. The centrifugal force causes the inner fluid to move towards the outer wall. The heat transfer from the outer wall would be higher than the inner wall because of two reasons; firstly, the occurrence of a higher fluid velocity (see sub-figure of figure 5) in the vicinity of the outer wall (see figure 5) and secondly, the appearance of secondary flow due to centrifugal force. Thus, it is expected that the transfer performances of bend pipes are better than that of straight pipes. A similar observation has been reported by Chandratilleke [39] while studying the convective heat transfer in a curved rectangular duct.
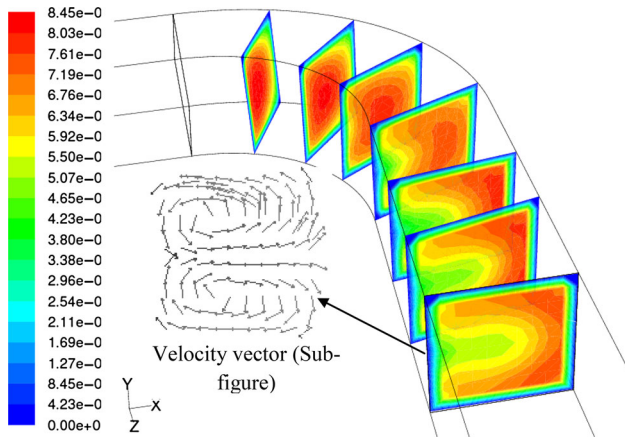
Figure 5. Velocity contours (m/s) for a square bend duct in different vertical planes for Al_2O_3−water nanofluid ($\phi = 1\%$, $Re_{Dh} = 3,000$).

It is interesting to note that a higher heat transfer enhancement is achieved for a higher volume fraction of the nanofluid (see figure 4). At $Re_{Dh} = 2,500$, the average Nusslet number has been increased by 9.6% as the nanofluid volume fraction is increased from 0% to 5%. However, at $Re_{Dh} = 6,000$, the heat transfer rate is increased by 12.3% as the volume fraction is increased from 0% to 5%. Since the heat transfer rate is augmented by the use of the nanofluid as compared to the conventional fluids such as water, it may be used for the thermal equipment where the heat elimination would be the prime objective.

5.3 *Effect of volume fraction of nanofluid on heat transfer enhancement*

Figure 6(a) shows the increase in Nusselt number with the nanofluid volume fraction. Al_2O_3-nano particles are added to the base fluid to form a homogeneous mixture. Two different Reynolds numbers have been considered for the

present analysis. At a particular volume fraction ($\phi = 5\%$), Nusselt number has been increased by 10.9% when the Reynolds number is increased from 5,000 to 6,000. Furthermore, at $Re_{Dh} = 5,000$ and 6,000, the heat transfer is enhanced by 10.34% and 10.2%, respectively, when a more nanoparticle by volume has been suspended in the base fluid (i.e., water). The heat transfer enhancement with the use of nanofluid is achieved because the thermal conductivity of the nanofluid is increased significantly which can carry heat effectively from the heated surface.

It has been evident from figure 6(b) that the turbulent kinetic energy (TKE) is increased with nanofluid volume fraction. The TKE is higher at the outer wall as compared to the inner wall. This is attributed to the centrifugal force experienced by the flow as it takes the curve. A peak in the TKE is seen at $AA/D_h = 22.2$ because of the secondary flow. The enhancement in TKE at outer wall is further explained from the velocity counter plots as shown in figure 7(a). At a particular $Re_{Dh} = 5,000$, the resultant velocity at the outer region of the wall is increased with the volume fraction; and hence, the turbulent kinetic energy is increased. The increased velocity along with high turbulence kinetic energy is responsible to dissipate more heat from the outer wall to the bulk fluid.

In figure 7(b), it is clear that the temperature gradient near the walls for $\phi = 4\%$ is higher than that of $\phi = 1\%$. Therefore, a more amount of heat is transferred from the wall to bulk fluid at higher volume fraction. Further, the particle–particle collision is intensified with the volume fraction of nanofluid; and thus, the fluid turbulence is increased. The intense collision can reduce the thermal boundary layer near the wall so as to facilitate the heat transfer to bulk fluid. Xuan and Li [9] proposed that the heat transfer enhancement was because of the intensification of turbulence due to the nanoparticles. Mansour *et al* [36] reported that the dimensionless thermal conductivity (k_{nf}/k_{bf}) of Al_2O_3–water nanofluid has been increased from 1 to 1.15, when the volume fraction of the nanofluid was
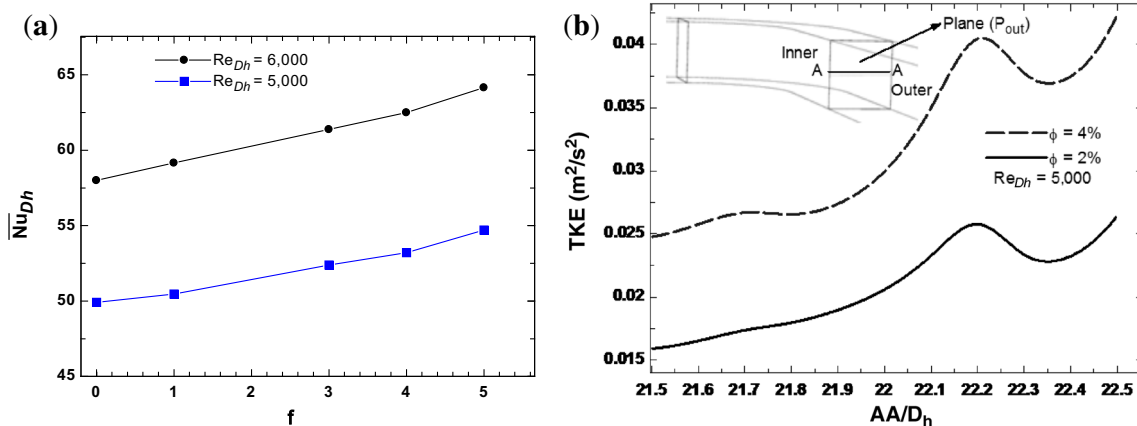

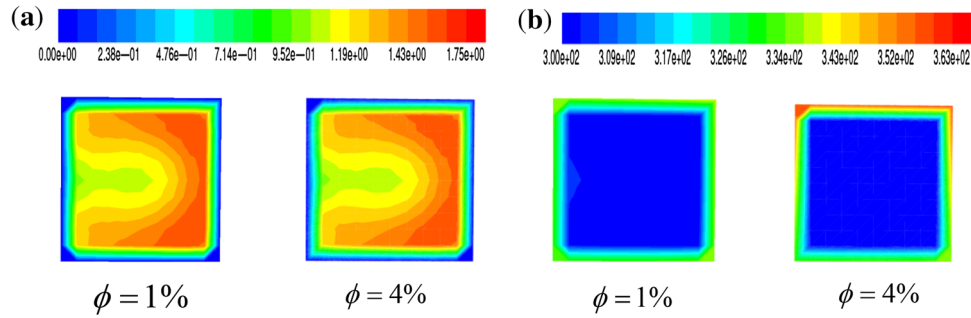**Figure 6.** (**a**) Variation of Nusselt number with nanofluid volume fraction; (**b**) Variation in TKE along the line AA.

Figure 7. Contours of (**a**) Velocity; (**b**) Temperature fields at $Re_{Dh} = 5{,}000$ in plane (i.e., P_{out}).
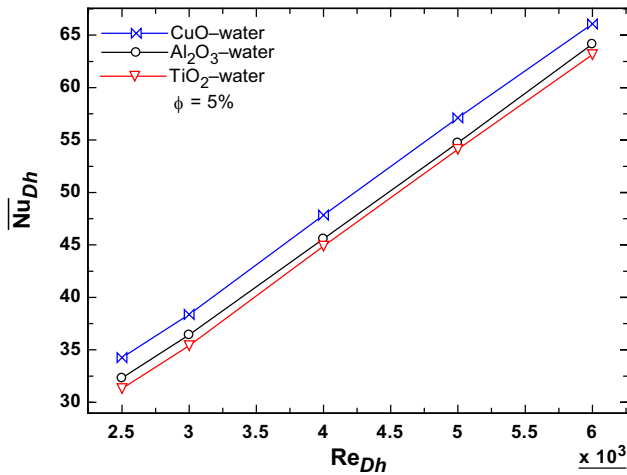

Figure 8. Variation of Nusselt number with duct Reynolds number for different nanofluids.

increased from 0% to 5%. In our present model, the dimensionless thermal conductivity is also improved from 1 to 1.14 as the volume fraction of the nanofluid is changed from 0% to 5%. It is worth mentioning here that the variation of nanofluid thermal conductivity with the volume fraction has been determined from Eq. (12).

5.4 *Effect of different water soluble nanofluids on heat transfer rate*

The effect of different types of nanofluid on heat transfer enhancement is shown in figure 8. The heat transfer by a particular type of nanofluid has been expressed in terms of area weighted Nusselt number. It is evident from figure 8 that the Nusselt number is increased linearly with Reynolds number as has already been discussed in section 5.2.

At a particular Reynolds number and the volume fraction of the nanofluid, the average Nusselt number of the CuO–water nanofluid is relatively higher than the other two types of the nanofluids (i.e., Al$_2$O$_3$–water and TiO$_2$–water). The higher Nusselt number of the CuO–water nanofluid is attributed to its higher thermal conductivity as compared to other two nanofluids considered. The present trend in the variation of the Nusselt number with Reynolds number employing different types of nanofluids is similar to the results reported by Abdolbaqi *et al* [40].

6. Conclusions

A three-dimensional computational domain has been solved numerically using the finite volume technique in order to investigate the heat transfer augmentation by nanofluids. Following conclusions can be drawn from the present study.

1. The area weighted average Nusselt number is found to increase linearly with the duct Reynolds number. At a particular duct Reynolds number (i.e., $Re_{Dh} = 6{,}000$), the heat transfer rate is increased by 12.3% as the volume fraction is increased from 0% to 5%.
2. At a particular volume fraction (phi = 5%), Nusselt number has been increased by 10.9% when the Reynolds number is increased from 5,000 to 6,000.
3. The secondary vortices observed the bend duct causes higher turbulence near the outer wall as compared to the inner wall. A higher velocity is also seen towards the outer wall.
4. The heat transfer augmentation with CuO nanofluid is observed to be higher than that of other two nanofluids (i.e., Al$_2$O$_3$ and TiO$_2$) considered in the present study. The numerical values of Nusselt number are observed to match well with the existing literature.

List of symbols

Dh	Hydraulic diameter of the rectangular duct (m)
C_p	Specific heat (J kg^{-1} K^{-1})
k	Thermal conductivity (W m^{-1} K^{-1})
u_{in}	Inlet velocity (m s^{-1})
u, v, w	Velocity in x-, y-and z-directions (m s^{-1})
P	Pressure (N m^{-2})

T_w	Wall temperature (K)
T_0	Inlet temperature (K)
T_b	Bulk mean temperature (K)
$\overline{Nu}_{Dh}$	Area weighted average Nusselt number
Re_{Dh}	Duct Reynolds number based on hydraulic diameter of the duct
q_w	Heat flux of isothermal surface (W m^{-2})

Greek symbols

ρ	Density (kg m^{-3})
μ	Kinematic viscosity (N s m^{-2})
ϕ	Volume fraction

Subscripts

w	Wall
b	Bulk
in	Inlet
bf	Base fluid
nf	Nanofluid

References

[1] Bejan A and Lorente S 2001 Thermodynamic optimization of flow geometry in mechanical and civil engineering. *J. Non-Equilibr. Thermodyn.* 26: 305–354

[2] Li Z, Mantel S C and Davidson J H 2005 Mechanical analysis of streamlined tubes with non–uniform wall thickness for heat exchangers. *J. Strain Anal. Eng. Des.* 40: 275–285

[3] Najafi H and Najafi B 2000 Multi-objective optimization of a plate and frame heat exchanger via genetic algorithm. *Heat Mass Transfer* 46: 639–647

[4] Ahuja A S 1975 Augmentation of heat transfer in laminar flow of polystyrene suspension. *J. Appl. Phys.* 46: 3408–3425

[5] Liu K V, Choi S U S and Kasza K E 1998 Measurement of pressure drop and heat transfer in turbulent pipe flows of particulate slurries. *Argonne National Laboratory Report* ANL-88-15

[6] Roco M C and Shook C A 1983 Modelling of slurry flow: the effect of particle size. *Canadian J. Chem. Eng.* 61:494–503

[7] Sohn C W and Chen M M 1981 Microconvective thermal conductivity in dispersed two-phase mixture as observed in low velocity Couette flow experiment. *J. Heat Transfer* 103: 47–51

[8] Choi S U S, Zhang Z G, Yu W, Lookwood F E and Grulke E A 2001 Anomalously thermal conductivity enhancement in nanotube suspension. *Appl. Phys. Lett.* 79: 2252–2254

[9] Xuan Y and Li Q 2000 Heat transfer enhancement with nanofluids. *Int. J. Heat Fluid Flow* 21: 58–64

[10] Wang X and Majumdar A S 2007 Heat transfer characteristics of nanofluids: A review. *Int. J. Therm. Sci.* 46: 1–19

[11] Kakaç S and Pramuanjaroenkij A 2009 Review of convective heat transfer enhancement with nanofluids. *Int. J. Heat Mass Transfer* 52: 3187–3196

[12] Xuan Y and Roetzel W 2000 Conceptions for heat transfer correlation of nanofluids. *Int. J. Heat Mass Transfer* 43: 3701–3707

[13] Roy G, Nguyen C T and Lajoje P 2004 Numerical investigation of laminar flow and heat transfer in a radial flow cooling system with use of nanofluids. *Superlattices Microstruct.* 35: 497–511

[14] Palm S J, Roy G and Nguyen C T 2006 Heat transfer enhancement with the use of nanofluids in radial flow cooling systems considering temperature-dependent properties. *Appl. Therm. Eng.* 26: 2209–2218

[15] Boungiorno J 2006 Convective transport in nanofluids. *J. Heat Transfer* 128: 240–250

[16] Rostamani M, Hosseinizadeh S F, Gorji M and Khodadadi J M 2010 Numerical study of turbulent forced convection flow of nanofluids in a long horizontal duct considering variable properties. *Int. Commun. Heat Mass Transfer* 37:1426–1431

[17] Anoop K B, Sundararajan T and Das S K 2009 Effect of particle size on the convective heat transfer in nanofluid in the developing region. *Int. J. Heat Mass Transfer* 52: 2189–2195

[18] Heris S Z, Esfahany M N and Etemad S G 2007 Experimental investigation of convective heat transfer of Al$_2$O$_3$/water nanofluid in circular tube. *Int. J. Heat Mass Transfer* 28: 203–210

[19] Wen D and Ding Y 2004 Experimental investigation into convective heat transfer of nanofluids at entrance region under laminar flow conditions. *Int. J. Heat Mass Transfer* 47: 5181–5188

[20] Heris S Z, Etemad S G and Esfahany M N 2006 Experimental investigation of oxide nanofluids laminar flow convective heat transfer. *Int. Commun. Heat Mass Transfer* 3: 529–535

[21] Seyf H R and Feizbakhshi M 2012 Computation analysis of nanofluid effects on convective heat transfer enhancement of micro-pin-fin heat sinks. *Int. J. Therm. Sci.* 58: 168–179

[22] Nazifard M, Nematollahi M, Jafarpur K and Suh K Y 2012 Numerical simulation of water-based alumina nanofluid in sub-channel geometry. *Sci. Technol. Nucl. Installat.* doi:10.1155/2012/928406

[23] Bianco V, Chiacchio F, Manca O and Nardini S 2009 Numerical investigation of nanofluids forced convection in circular tubes. *Appl. Therm. Eng.* 29: 3632–3642

[24] Heris S Z, Nassan T H, Noie S H, Sardarabadi H and Sardarabadi H 2013 Laminar convective heat transfer of Al$_2$O$_3$/water nanofluid through square cross section duct. *Int. J. Heat Fluid Flow* 44: 375–382

[25] Lotfi R, Saboohi Y and Rashidi A M 2010 Numerical study of forced convective heat transfer heat transfer of nanofluids: Comparison of different approaches. *Int. Commun. Heat Mass Transfer* 37: 74–78

[26] Azari A, Kalbasi M and Rahimi M 2014 CFD and experimental investigation on the heat transfer characteristics of alumina nanofluids under the laminar regime. *Braz. J. Chem. Eng.* 31: 469–481

[27] Maiga S E B, Palm S J, Nguyen C T, Roy G and Galanis N 2005 Heat transfer enhancement by using nanofluids in forced convection flows. *Int. J. Heat Fluid Flow* 26: 530–546

[28] Launder B E and Spalding D B 1974 The numerical computation of turbulent flows. *Comput. Meth. Appl. Mech. Eng.* 3: 269–279

[29] Barik A K, Dash S K and Guha A 2015a Experimental and numerical investigation of air entrainment into an infrared suppression device. *Appl. Therm. Eng.* 75: 33–44

[30] Barik A K, Dash S K and Guha A 2015b Entrainment of air into an infrared suppression device (IRS) using circular and non-circular multiple nozzles. *Comput. Fluids* 114: 26–38

[31] Choi J and Zhang Y 2012 Numerical simulation of laminar forced convective heat transfer of Al_2O_3-water nanofluid in a pipe with return bend. *Int. J. Therm. Sci.* 55: 90–102

[32] Akbarinia A and Behzadmehr A 2007 Numerical study of laminar mixed convection of nanofluid in horizontal curved tubes. *Appl. Therm. Eng.* 27: 1327–1337

[33] Pak B C and Cho Y I 1998 Hydrodynamic and heat transfer study of dispersed fluids with submicron metallic oxide particles. *Exper. Heat Transfer* 11: 151–170

[34] Maiga S E B, Nguyen C T, Galanis N and Roy G 2004 Heat transfer behaviours of nanofluids in a uniformly heated tube. *Superlattices Microstruct.* 35: 543–557

[35] Lee S, Choi S U S, Li S and Eastman J A 1999 Measuring thermal conductivity of fluids containing oxide nanoparticles. *J. Heat Transfer* 121: 280–289

[36] Mansour R B, Galanis N and Nguyen C T 2007 Effect of uncertainties in physical properties on forced convection heat transfer with nanofluids. *Appl. Therm. Eng.* 27: 240–249

[37] Muralidhar K and Biswas G 2005 *Advanced engineering fluid mechanics*. Norosa Publishing House, New Delhi

[38] Chakraborty G 2008 A note on methods for analysis of flow through microchannels. *Int. J. Heat Mass Transfer* 51: 4583–4588

[39] Chandratilleke T T and Nursubyakto 2003 Numerical prediction of secondary flow and convective heat transfer in externally heated curved rectangular ducts. *Int. J. Therm. Sci.* 42: 187–198

[40] Abdolbaqi M K, Azwadi C S N and Mamat R 2014 Heat transfer augmentation in the straight channel by using nanofluids. *Case Stud. Therm. Eng.* 3: 59–67